The Baltic Sea Tracer Release Experiment: 1. Mixing rates

Peter L. Holtermann,[1] Lars Umlauf,[1] Toste Tanhua,[2] Oliver Schmale,[1] Gregor Rehder,[1] and Joanna J. Waniek[1]

Received 8 July 2011; revised 3 November 2011; accepted 8 November 2011; published 28 January 2012.

[1] In this study, results from the Baltic Sea Tracer Release Experiment (BATRE) are described, in which deep water mixing rates and mixing processes in the central Baltic Sea were investigated. In September 2007, an inert tracer gas (CF_3SF_5) was injected at approximately 200 m depth in the Gotland Basin, and the subsequent spreading of the tracer was observed during six surveys until February 2009. These data describe the diapycnal and lateral mixing during a stagnation period without any significant deep water renewal due to inflow events. As one of the main results, vertical mixing rates were found to dramatically increase after the tracer had reached the lateral boundaries of the basin, suggesting boundary mixing as the key process for basin-scale vertical mixing. Basin-scale vertical diffusivities were of the order of 10^{-5} m^2 s^{-1} (about 1 order of magnitude larger than interior diffusivities) with evidence for a seasonal and vertical variability. In contrast to tracer experiments in the open ocean, the basin geometry (hypsography) was found to have a crucial impact on the vertical tracer spreading. The e-folding time scale for deep water renewal due to mixing was slightly less than 2 years, the time scale for the lateral homogenization of the tracer patch was of the order of a few months.

Citation: Holtermann, P. L., L. Umlauf, T. Tanhua, O. Schmale, G. Rehder, and J. J. Waniek (2012), The Baltic Sea Tracer Release Experiment: 1. Mixing rates, *J. Geophys. Res.*, *117*, C01021, doi:10.1029/2011JC007439.

1. Introduction

[2] Tracer Release Experiments (TREs) conducted with the long-term stable compounds SF_6, and more recently CF_3SF_5, have evolved over the last 2 decades as a useful alternative technique for quantifying the integral effect of mixing in the ocean and in lakes [*Watson and Ledwell*, 2000; *Ho et al.*, 2008; *Ledwell et al.*, 2011]. Beyond the diapycnal and isopycnal mixing rates that can be inferred from the spreading behavior of the tracer, in many cases TREs have also helped identifying the physical key processes responsible for mixing. Examples are the TREs conducted in stratified ocean basins [*Ledwell and Bratkovich*, 1995; *Ledwell and Hickey*, 1995], fjords [*Stigebrandt*, 1979] and lakes [*Goudsmit et al.*, 1997] that have shown strong evidence for the importance of boundary mixing processes.

[3] Here, we report results from the Baltic Sea Tracer Release Experiment (BATRE) during which deep water mixing in the Baltic Proper was studied. Mixing in this part of the Baltic Sea is known to determine the vertical transport of nutrients, in particular phosphate and dissolved trace metals from the deep, usually anoxic layers, therefore constituting an essential component of the basin-scale nutrient cycle with considerable implications for ecosystem functioning [*Feistel et al.*, 2008; *Reissmann et al.*, 2009]. Previous studies have shown that some information about the effective basin-scale diffusivities may be inferred from the construction of deep water budgets for heat and salt [e.g., *Axell*, 1998]; for O_2, PO_4 and NH_4 [*Gustafsson and Stigebrandt*, 2007]; and for CO_2 [*Schneider et al.*, 2010]. These methods, however, involve large uncertainties introduced by additional model assumptions required to compensate for the nonconservative properties of some of the tracers, and to quantify deep water renewal due to advective effects ("inflow events"). The only deep diapycnal mixing experiment with a deliberately released, conservative tracer conducted in the Baltic Sea we are aware of is the dye study described by *Kullenberg* [1977], which, however, focused on completely different time scales (a few days), and was conducted in a different area.

[4] Besides the problem of a precise quantification of deep water mixing rates, approaches based on the construction of volume-averaged deep water budgets are, by their nature, not a useful tool for identifying mixing processes and flux pathways of matter. In spite of numerous suggestions, these processes are at the moment only poorly understood. As one possibility, *Axell* [1998] speculated that, similar to the open ocean, internal wave mixing determines deep water mixing in the Baltic Sea. Conclusive evidence for this, however, is so far missing, in particular in view of the fact that internal tides as one of the most important mixing processes in the ocean are absent in the Baltic Sea.

[1]Leibniz Institute for Baltic Sea Research, Warnemunde, Germany.
[2]Leibniz Institute for Marine Sciences, Kiel, Germany.

0148-0227/12/2011JC007439

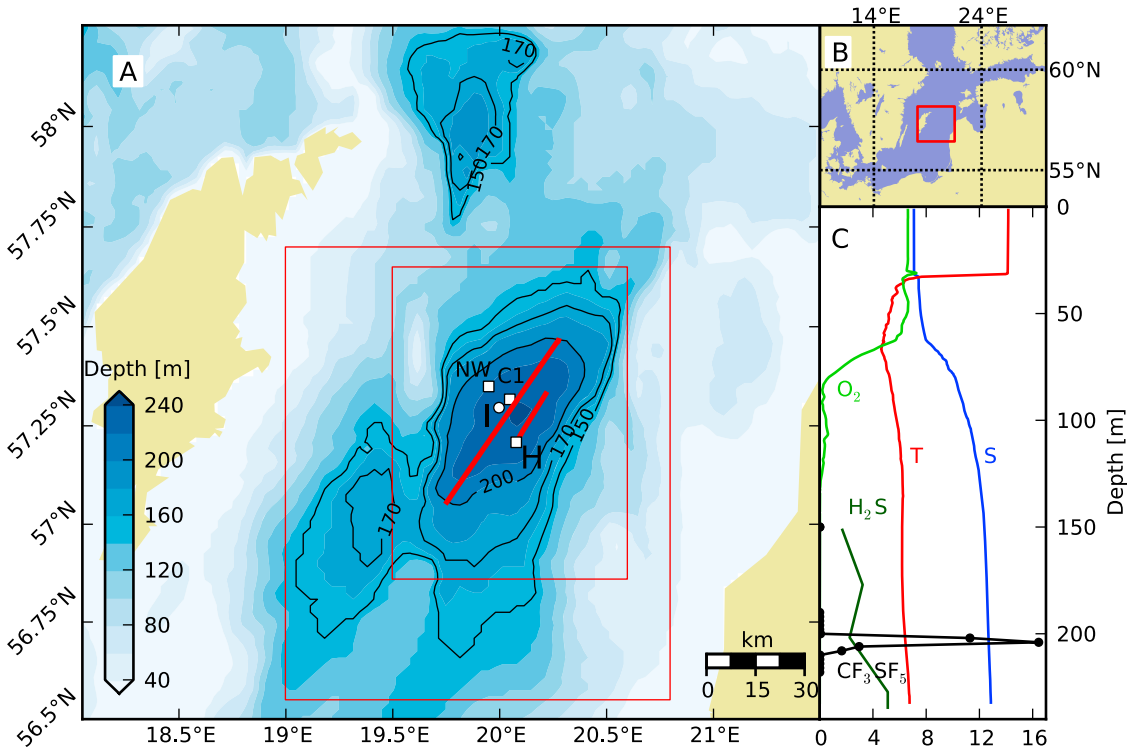

Figure 1. (a) Gotland Basin with red rectangles marking subareas shown in later figures. "I" indicates the tracer injection, "H" the position where tracer was first detected. "NW" and "C1" denote positions of two moored current meters. Pump-CTD tracks are shown as red lines. (b) Overview map with study area marked in red; (c) CTD profile taken on 24 September 2007 at position H with salinity (g kg^{-1}), temperature (°C), oxygen (ml l^{-1}), and the tracer concentration (10 pmol kg^{-1}). The H_2S (10 μmol kg^{-1}) profile was taken at the 31 August 2007 at station C1.

[5] This work is split into two parts, of which this paper contains the description of the tracer experiment, and the analysis of the basin-scale mixing rates. The physical processes responsible for the observed mixing rates are analyzed in the companion paper by *Holtermann and Umlauf* [2012, hereinafter Part 2]. A brief description of the tracer injection is given by *Umlauf et al.* [2008].

2. Study Site

[6] The study area for all measurements conducted in the framework of BATRE is the Gotland Basin, the largest of the deep basins of the Baltic Sea (Figure 1). Located in the center of the Baltic Proper, the Gotland Basin has a maximum depth of approximately 240 m, and a lateral scale of the order of 100 km. For the interpretation of the lateral tracer spreading it is important to note that the 170 m isobath defines the lateral extent of the Gotland Basin, while the 150 m isobath includes both the Gotland Basin and the shallower southwestern side basin, both connected by a sill at 165 m depth. Even shallower is a sill at approximately 130 m depth, connecting the Gotland Basin with the Fårö Deep in the north (Figure 1a).

[7] The hydrographic parameters measured on 24 September 2007, approximately 2 weeks after the tracer injection, represent typical late summer conditions in the Gotland Basin (Figure 1c). Below the seasonal thermocline at approximately 30 m depth, the stability of the water column is almost exclusively determined by vertical salinity gradients with a particularly stable halocline located around 80 m depth. The slightly increasing temperatures toward the bottom indicate a weak deep water inflow that had occurred between April and August 2007, just before the tracer injection as described in more detail below. Data from our moored instrumentation described in Part 2, as well as results from the regular monitoring cruises conducted by the Leibniz Institute for Baltic Sea Research (IOW), suggest that after this inflow event no significant deep water renewal occurred until the end of the experiment in February 2009. Our data set therefore represents deep water mixing during a well-defined physical regime (stagnation period), which greatly facilitates the interpretation of the tracer spreading rates.

[8] The appearance of the anoxic region below approximately 130 m depth (Figure 1c) is a typical feature observed during stagnation periods, known to have considerable consequences for the deep water biogeochemistry and microbiology. Under such conditions, the deep layers typically exhibit high concentrations of H_2S (Figure 1c) due to sulphate reduction with associated fluxes of phosphate from the sediments, and recycling of trace metals like Fe and Mn [*Feistel et al.*, 2008]. The exchange between the anoxic deep layers and the upper mixed layer is of central importance for

Table 1. Summary of the BATRE Cruises[a]

Survey	Cruise	Vessel	Date	CTD	CF_3SF_5	MSS
Preinjection	P353	R/V *Poseidon*	16–19 July 2007	4	39	–
Injection	P357A	R/V *Poseidon*	9–14 September 2007	40	1	226
Leg 1	P357B	R/V *Poseidon*	21–24 September 2007	PCTD	PCTD	–
Leg 2	PE0725	R/V *Prof. A. Penck*	25–31 October 2007	64	363	234
Leg 3	AL312	R/V *Alkor*	28 Jan to 5 February 2008	32	429	97
Leg 4/1	MSM0803	R/V *Merian*	27 June 2008	5	22	–
Leg 4/2	P370	R/V *Poseidon*	9–15 August 2008	3	22	–
Leg 5	AL331	R/V *Alkor*	5–9 February 2009	33	242	–

[a]Dates include only the duration of actual measurements in the Gotland Basin. Last three columns indicate the number of CTD stations, tracer samples, and microstructure casts with the MSS profiler, respectively.

the ecosystem, in particular for primary production, and has motivated the tracer study described in the following.

3. Methods

3.1. Tracer and Injection System

[9] The tracer used in BATRE is trifluoromethyl sulfur pentalfluoride (CF_3SF_5), a compound selected as a replacement for SF_6 that has traditionally been used in TREs [*Ho et al.*, 2008]. The main motivation for the use of CF_3SF_5 in tracer release experiments is to avoid contaminating the ocean with deliberately released SF_6 ensuring that this tracer can serve also in the future as an oceanic transient tracer with the atmosphere as the only source. The physical and chemical properties of CF_3SF_5 are summarized by *Ho et al.* [2008].

[10] In a pilot study in the Santa Monica Basin off the Californian coast recently described by *Ho et al.* [2008], a mixture of SF_6 and CF_3SF_5 was simultaneously injected. Nearly identical spreading rates of the two tracers were observed, suggesting CF_3SF_5 as a viable alternative to SF_6 in oceanic tracer experiments. Moreover, in the absence of any significant natural and industrial sources, or any previous tracer experiments with CF_3SF_5, we expect that before BATRE the background concentrations of CF_3SF_5 were below the detection limit everywhere in the Baltic Sea. We have explicitly verified this by measurements of profiles from 3 stations in the Gotland Basin sampled on 16–18 July 2007, i.e., about 2 months prior to the injection of the tracer.

[11] For the tracer injection, we used a towed Ocean Tracer Injection System (OTIS), similar to the instruments described for previous tracer studies [*Ledwell and Bratkovich*, 1995; *Ledwell et al.*, 1998; *Ho et al.*, 2008; *Ledwell et al.*, 2011]. With the help of the OTIS, the tracer was sprayed in the form of liquid droplets through two 25 μm orifices into the water column, while the instrument frame was towed behind the ship at approximately 1 kn inside a predefined density range. Outside of this range, e.g., during the descend to the target density, an inert primer fluid (Vertrel XF) was slowly flushed through the orifices in order to avoid clogging.

3.2. Oceanographic Instrumentation

[12] On all cruises (Table 1), except the first tracer survey, tracer samples were taken with 10 l free flow bottles from Hydro-Bios (Germany), attached to a standard CTD rosette. O rings were removed from the bottles, cleaned in isopropanol, and degassed in a vacuum oven prior to use due to a possible affinity of the tracer to rubber materials. Hydrographic variables were obtained using a SBE 911plus CTD package (Sea-Bird, USA), equipped with freshly calibrated double sensors for temperature and conductivity, except for the injection cruise where only a single set of sensors was available. The accuracy of the sensors is 0.001° C for temperature and 0.001 g kg^{-1} for salinity.

[13] During the first tracer survey (Leg 1; tracer surveys are referred to as "Legs" in the following), when the tracer distribution was still very streaky, we used a pumped CTD system (PCTD) for the tracer sampling. The PCTD consists of a small CTD frame (without Rosette), equipped with double SBE 911plus sensors, and a high-pressure pump connected to the onboard wet lab via a nylon hose embedded in a multifunction cable [*Strady et al.*, 2008]. This instrument was towed behind the ship at a specified density level, thus providing a continuous stream of water samples representing the isopycnal distribution of the tracer. In combination with the equilibrator system for on-line tracer analysis described in section 3.3 below, this turned out to be a useful tool for the detection of intermittent tracer patches during the initial stages of the experiment.

[14] In addition to the ship-based measurements, a set of moorings was deployed in the Gotland Basin. In this paper, we only discuss velocity records from the northwest (NW) and central (C1) moorings with the locations shown in Figure 1a. These instruments are described in more detail in Part 2.

3.3. Analytical Systems for Tracer Analysis

[15] Tracer measurements were generally performed onboard using up to 3 purge and trap gas chromatographic measurement systems similar to the one described by *Bullister and Weiss* [1988], modified in the following way to optimize the analysis of CF_3SF_5. Due to the presence of H_2S in the water column, we used a column filled with Ascarite after the desiccant to scrub the H_2S out of the gas flow, which would otherwise obscure the tracer peaks in the chromatogram. For trapping, we used a 12 cm long 1/8″ SS tube packed with HayeSep D cooled to −30°C, followed by desorption at 120°C onto a 15–30 cm long Porasil C 1/8″ precolumn. The CF_3SF_5 and CFC-12 were passed on to the main column: 180 cm Carbograph 1AC (60–80 mesh) followed by 20 cm Molsieve 5A. Detection was performed on an Electron Capture Detector. Standardization was done by injection of gaseous standards calibrated using a commercial standard (accuracy claimed by the company is 10%). The CFC-12 data were used to check for incorrectly closed CTD bottles or other analytical problems; large deviations of the CFC-12 concentration from the bulk of the samples

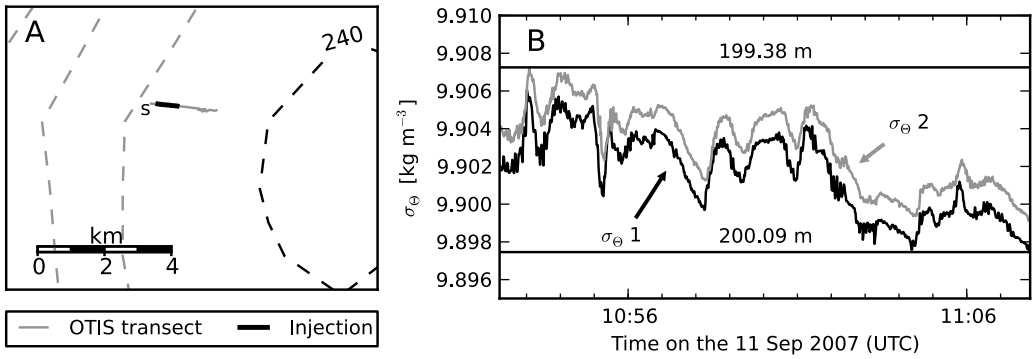

Figure 2. (a) Injection track near position I (see Figure 1) and (b) potential density variation during the injection with data from two simultaneously operated CTD systems on the OTIS.

normally indicated a problem, and the CF_3SF_5 values were flagged accordingly.

[16] During the surveys where we brought the instruments to sea, water samples with ground glass syringes either from the CTD bottles or from the continuous flow from the PCTD were collected. Only for the preinjection survey and Leg 4 (Table 1), approximately 120 ml samples were collected in 150 ml glass ampules that were flame sealed on the ship and later measured in the institutes' labs. For Leg 1 we additionally used a "shower head" equilibrator connected to the continuous flow from the PCTD from which a flow rate of approximately 2 l/min was maintained through the equilibrator. Every 6 min a 12 ml sample of the circulating air was drawn from the equilibrator, which was trapped, desorbed and analyzed as a normal standard on the gas chromatograph. The equilibrator proved to be an excellent indicator for the presence of tracer in the waters along the cruise track. However, due to the large carry over effect of the equilibrator, this setup was a poor indicator for when we left the tracer patch. During Leg 1, the equilibrator was complemented by two analytical systems leading to a sampling rate of about 1 sample in 3 min along the cruise track. An intercomparison of the two instruments proved the consistency of the data.

3.4. Stability Test of CF_3SF_5 in Anoxic Seawater

[17] Several volatile halogenated compounds are known to degrade in anoxic conditions; for instance, CFC-11 and CCl_4, whereas CFC-12 appears to be stable [*Bullister and Lee*, 1995; *Krysell et al.*, 1994; *Tanhua et al.*, 1996; *Tanhua and Olsson*, 2005]. However, no studies have so far been conducted to determine the stability of CF_3SF_5 in anoxic seawater. Since the water of the Gotland Basin becomes anoxic at about 130 m depth (Figure 1c), any degradation of the tracer under these conditions would have influenced our experiment. We therefore conducted a long-term stability test; during Leg 3 of the experiment (January 2007, about 4 months after injection) 12 ampoules were filled, and subsequently flame sealed, from 7 different Niskin bottles that were triggered at the density of 9.9 kg m^{-3} (corresponding to approximately 210 m depth). The concentration of CFC-12 and CF_3SF_5 was measured immediately during the cruise, and subsets of the ampoules were subsequently measured in the lab 593, 897 and 1344 days after sampling. The ampoules, with a volume of about 125 ml, were completely filled and flushed with 3 additional volumes. A headspace of clean N_2 gas was introduced in the lab prior to flame sealing so that 100–110 ml of water remained in the ampoule. The measured concentrations of CFC-12 and CF_3SF_5 did not show any significant trends over the 3.7 years of the experiment. Similarly, we did not find any trend in the SF_6 concentration between day 593 and day 1344 of the experiment. This indicates that the commonly used transient tracers SF_6 and CFC-12 and the deliberately released tracer CF_3SF_5 are all stable in anoxic seawater.

4. Ship-Based Measurements

4.1. Tracer Injection

[18] The tracer injection took place on 11 September 2007 at the central position I in the eastern Gotland Basin during a cruise with R/V *Poseidon* (Figure 1). The amount of 0.9 kg (4.6 mol) of CF_3SF_5 was injected as a single streak of approximately 1 km length (Figure 2a) inside a small density interval around the target isopycnal (potential density: 9.9 kg m^{-3}) as verified by the two independent CTD loggers mounted on the instrument frame. The small uncertainty in the injection density corresponds to less than 1 m vertical variability around the injection level at approximately 200 m depth (see Figure 2b). As in other experiments of this type, it is likely that the finite time required for the full dissolution of the tracer droplets results in a small amount of tracer sinking, and that the turbulent wake behind the injection system leads to some vertical mixing of the tracer plume. These effects are hard to quantify but the results from the first tracer survey described below suggest that neither did have a significant impact on the vertical tracer dispersion on longer time scales.

4.2. Tracer Surveys

[19] After the injection cruise in September 2007, the spreading of the tracer was observed during six tracer surveys conducted between September 2007 and February 2009 with some of these cruises also including turbulence microstructure measurements as described in Part 2 (Table 1 and Figure 3). Here and in the following, DAI (days after injection) denotes the number of days elapsed between the tracer injection (11 September 2007) and the first tracer profile obtained during the tracer surveys, respectively. All times are reported in UTC.

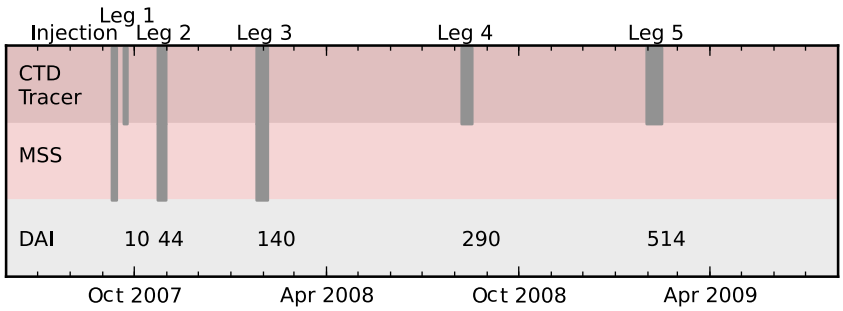

Figure 3. Time line of BATRE project cruises with type of available data (CTD, CF_3SF_5, microstructure with MSS profiler) as indicated. Days between injection (DAI), are days after 11 September 2007 and the first CTD measurement inside the Gotland Basin, respectively.

4.2.1. Leg 1

[20] Approximately 2 weeks after the injection, R/V *Poseidon* returned to the Gotland Basin for first tracer survey (Leg 1) starting on 21 September 2007. In view of the anticipated streakiness of the tracer at this early stage of the experiment, we used a special sampling strategy. Continuous water samples taken from the PCTD were instantaneously analyzed with the equilibrator system described above, while the CTD frame was slowly towed along the target isopycnal, following two cross-basin transects inside the 200 m isobath (Figure 1a). No significant tracer signals were found until 24 September 2007, when the tracer patch was first detected near position H. Subsequent vertical tracer profiling with the PCTD at this position revealed a narrow tracer distribution with peak concentrations above 160 pmol kg^{-1} at a density of approximately $\sigma_\theta = 9.92$ kg m^{-3}, i.e., slightly larger than the injection density. This points at a small amount of sinking, probably during the injection as outlined above. A cast taken immediately after the recovery of the PCTD with the CTD Rosette system did not hit the tracer patch again. Limited by available ship time, the tracer survey had to be discontinued but the results from Leg 1 were sufficient to draw the following conclusions: (1) the tracer was injected at the intended target isopycnal, (2) tracer sinking and tracer mixing in the wake of the OTIS were small, and turned out to be insignificant compared to the spreading rates observed during later surveys, (3) advection has transported the tracer patch at least 10 km to the southeast within 11 days, and (4) the tracer distribution on the target isopycnal was found to be extremely inhomogeneous.

4.2.2. Legs 2–5

[21] Leg 1 was followed by 5 additional tracer surveys that were, except for Leg 4 discussed below, carried out following a similar pattern. Table 1 includes a complete listing of the tracer surveys, and Figure 3 shows the time line of the experiment. For Legs 2, 3, and 5, the region of interest was covered with a regular station grid (see Figures 10 and 13), on which bottle samples were taken with the CTD rosette system. Samples were analyzed onboard within approximately 60 min, using the purge-and-trap system described in section 3.3. This waiting time was often used for microstructure measurements at the same location, yielding 4 or 5 full depth profiles per tracer station as described in more detail in Part 2. The two cruises in summer 2008 with R/V *Merian* (Leg 4/1) and R/V *Poseidon* (Leg 4/2) were mostly dedicated to other research projects, and only a few tracer profiles, and no turbulence profiles, were obtained. Since no analytical system was on board, tracer samples were sealed into glass ampules, and later analyzed in the institute's laboratory. Due to the low mixing rates in summer and the small temporal separation between the two surveys, tracer profiles in the center of the basin were found to have nearly identical shapes (see below), and we decided to discuss them jointly as Leg 4.

5. Conversion Between Potential Density and Depth

[22] An important step in the analysis of vertical mixing with the help of an isopycnically averaged transport equation for the tracer concentration is the introduction of a representative mapping between potential density and depth. In the presence of bounding topography and a strong variability of isopycnal surfaces (Part 2) this is not a trivial task. *Winters et al.* [1995] showed that isopycnal displacements due to reversible (e.g., internal wave) motions can be separated from irreversible changes due to mixing by adiabatically sorting the instantaneous density field into a state of minimum ("background") potential energy. While this method has frequently been applied for the interpretation of model data, a direct application to field data is complicated by the fact that synoptic data with sufficient resolution are rarely available.

[23] Here, we have investigated three different approaches, each with relative merits and disadvantages, in order to separate reversible from irreversible isopycnal motions by approximating the vertical distribution of the density in the sorted background state. The most obvious approach is based on the assumption that the density profile at the deepest point of the basin represents the background state. By definition, this method has the advantage that the full depth range is included in the conversion between depth and density. However, the maximum density is often not observed at the deepest point of the basin, implying that tracer samples taken at higher densities are not included in the analysis. This problem can be overcome by interpreting the *densest* profile as the profile representing the sorted state. However, as illustrated in Figure 4 showing all available density profiles for Legs 1–5, with this approach the lowest part of the water column is not included. In some cases (e.g., for Leg 3), this loss of data corresponds to a substantial fraction of the lower water column.

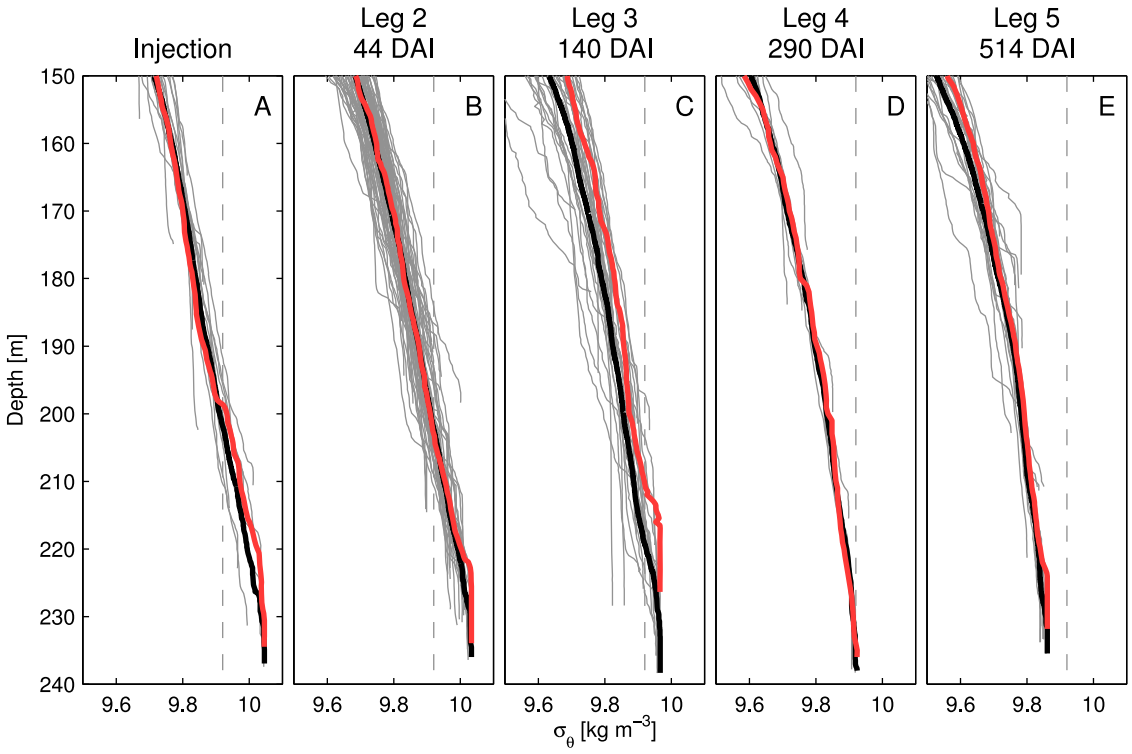

Figure 4. Potential density observed during the injection and the tracer surveys (Legs 2–5). Gray indicates all available profiles. Red indicates densest profile. Black indicates sorted profile (see section 5). Dashed gray indicates injection density.

[24] As a useful alternative, here we suggest the following approximation for the background density field that, as the original method of *Winters et al.* [1995], is based on sorting. Potential density profiles taken at the lateral positions $\mathbf{x}_j$ are interpolated onto a set of standard depths z_i with vertical spacing $\Delta z = 1$ m. We assign the volume $\Delta V_j = \Delta z \Delta A_j$ to each point in this grid, where ΔA_j corresponds to the horizontal area represented by the CTD profile taken at position $\mathbf{x}_j$. Practically, we identify ΔA_j with the area of Voronoi cells found from a so-called Voronoi decomposition of the CTD grid. The mathematical method is described by *Barber et al.* [1996]; some examples for Voronoi decompositions of Leg 2 and Leg 3 are shown in Figure 5.

[25] Using the hypsographic area $A(z)$ of the basin, the background density field is found by monotonically sorting the measured densities along the new vertical coordinate z^*. Using this method, each original density estimate obtained at lateral position $\mathbf{x}_j$ and depth z_i is assigned a new (sorted) vertical position z_{ij}^*. The original volumes ΔV_j (and hence the total volume) are retained, provided the vertical depth interval Δz_{ij}^* in the sorted state obeys the relation $\Delta z_{ij}^* A(z_{ij}^*) = \Delta z \Delta A_j$.

[26] Clearly, this method is only an option if a sufficient number of CTD profiles is available, and if it is assumed that ship surveys represent a synoptic picture of the density field, which is only satisfied in an approximate sense here. Sorted density profiles for all cruises are shown in Figure 4, together with the original density profiles on which the sorting was based on. In spite of the practical imperfections outlined above, it is evident that the sorting approach retains two important properties of the original method by *Winters et al.* [1995]: it includes both the full depth range and the full density range, different from the two simple approaches outlined above. For these reasons, the mapping between depth and potential density discussed in the following will be based on sorting, unless otherwise noted.

6. Observation of Tracer Spreading

[27] All tracer samples obtained during Legs 2–5 are summarized in Figures 6–9 as functions of potential density,

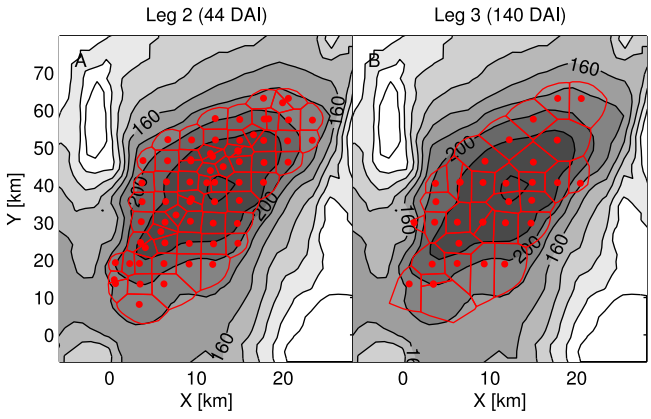

Figure 5. Locations of CTD casts (red dots) for (a) Leg 2 and (b) Leg 3 and corresponding Voronoi cells used for the density sorting algorithm described in section 5.

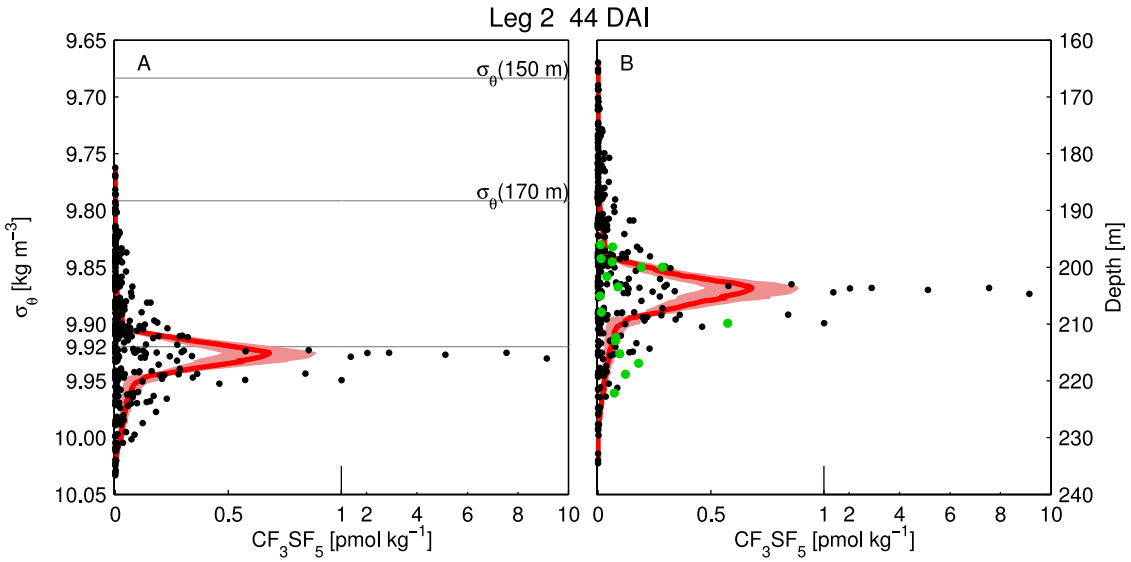

Figure 6. Tracer distribution for Leg 2 plotted (a) versus potential density and (b) versus depth in the sorted reference state (see section 5). Note the change of scale at 1 pmol kg^{-1}. Average profile in red, uncertainty in light red. Horizontal lines in Figure 6a mark selected depth levels discussed in the text. Green dots in Figure 6b denote near-bottom nonzero tracer samples (taken within 2 m distance from the bottom).

and, using the algorithm described above, as functions of depth. Isopycnal averages were evaluated in discrete form as the volume average of the tracer concentrations between two isopycnal surfaces with potential densities σ_θ and $\sigma_\theta + \Delta\sigma_\theta$, respectively, where we used a constant spacing of $\Delta\sigma_\theta = 0.01$ kg m^{-3} in density space.

[28] Due to the small number of tracer profiles this approach was not applicable for Leg 4; instead, for this data set, we used the weighted averaging method described by *Ledwell and Bratkovich* [1995]. An overview over the lateral distribution of the tracer during Legs 2–5 is given in Figure 10, showing the average tracer concentration below the 150 m isobath that encloses the basin and its southwestern appendix (Figure 1). The isopycnal distribution of the tracer for Legs 2–5 is illustrated in Figure 11, where, as an example, isopycnals located in the vicinity of the injection level (approximately 200 m depth) have been chosen.

6.1. Tracer Spreading in the Gotland Basin

[29] Figures 10a and 11a illustrate that during Leg 2 (44 DAI) the lateral tracer distribution was still extremely inhomogeneous, which is also evident in the isopycnal scatter shown in Figure 6. Nearly all of the tracer profiles peak at 9.92 kg m^{-3}, suggesting that no further tracer sinking had occurred after Leg 1. Tracer concentrations above 170 m depth are negligible, and we expect that no tracer has left the central Gotland Basin at this early stage of the experiment. Moreover, Figures 10a and 11a suggest that the

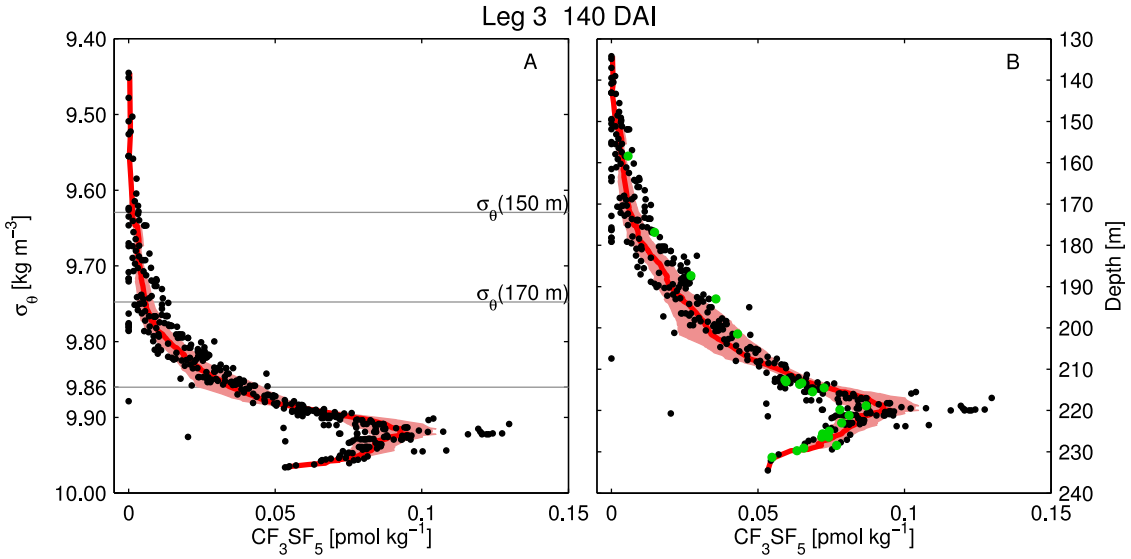

Figure 7. As in Figure 6 but for Leg 3.

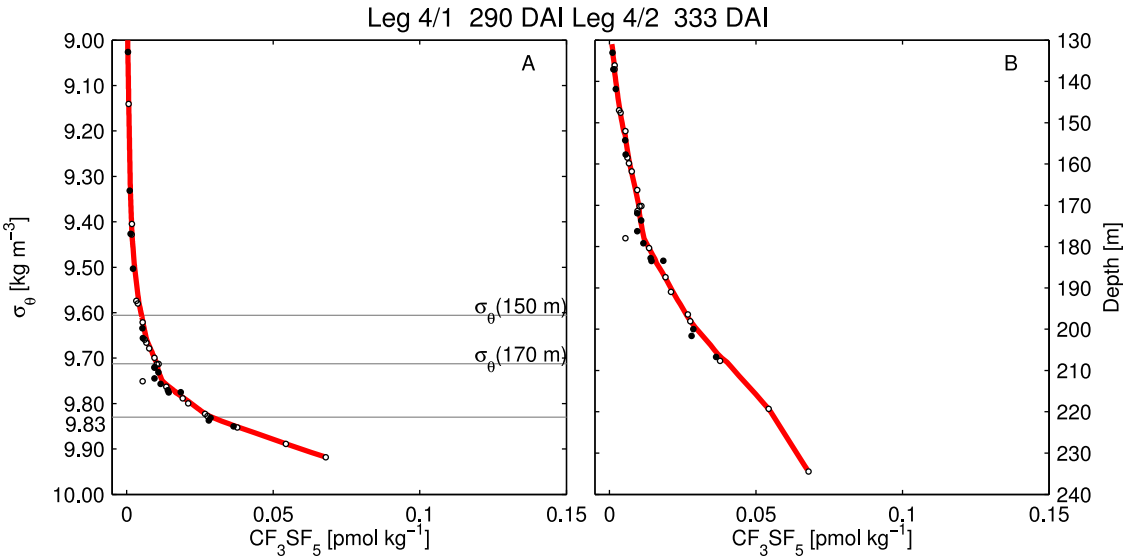

Figure 8. As in Figure 6 but for Leg 4. Open circles show the tracer samples for Leg 4/1 (June 2008) and solid circles show the tracer samples for Leg 4/2 (August 2008).

tracer patches have not been in intense contact with the lateral slopes of the basin, which will be important for the distinction between interior and boundary mixing processes. Nevertheless, in some of the near-bottom samples (green markers in Figure 6b) small amounts of tracer were found, pointing at a starting influence of boundary mixing. We will come back to this point below.

[30] In view of the observed patchiness, it is not unlikely that advection of small-scale tracer patches has resulted in double counting of the same tracer at different grid points during the survey. To investigate this aspect more closely, the exact sampling dates as well as the pseudotrajectories computed from the current records at moorings C1 and NW are summarized in Figure 12. These data let us suspect that, indeed, some tracer patches were measured twice. For example, the pseudotrajectories at C1 and NW marked in gray suggest that the patch with the highest concentrations measured on 25 October (18:18) could have been advected southward during the following 2.9 days, and was resampled a second time, at least partly, on 28 October (16:46) approximately 5 km southeast (Figure 12). Similarly, it is likely that the northern patch, first sampled on 26 October (23:09), was resampled 17 hours later on 27 October (16:16), a few kilometers south (the corresponding section of the trajectories is colored in red). The implications of this double counting for the construction of the basin-scale tracer budget will be discussed in more detail below.

[31] The tracer concentrations during the following Legs 3–5 (Figures 7–9) reveal a strong reduction of isopycnal scatter compared to Leg 2, consistent with the comparably homogeneous lateral tracer distributions shown in Figures 10 and 11. Already for Leg 3 (140 DAI), lateral dispersion

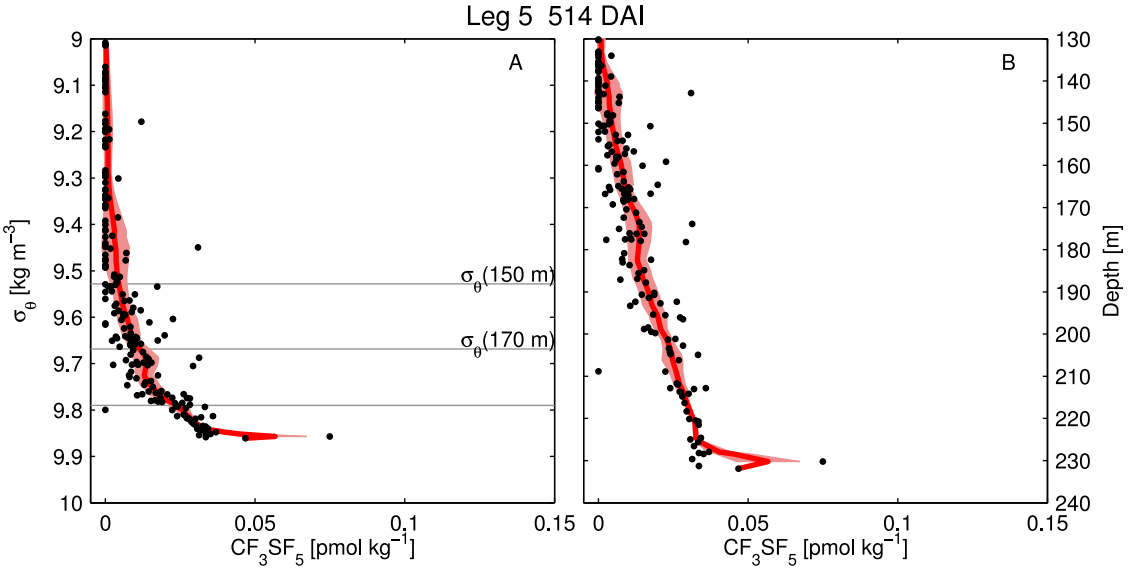

Figure 9. As in Figure 6 but for Leg 5.

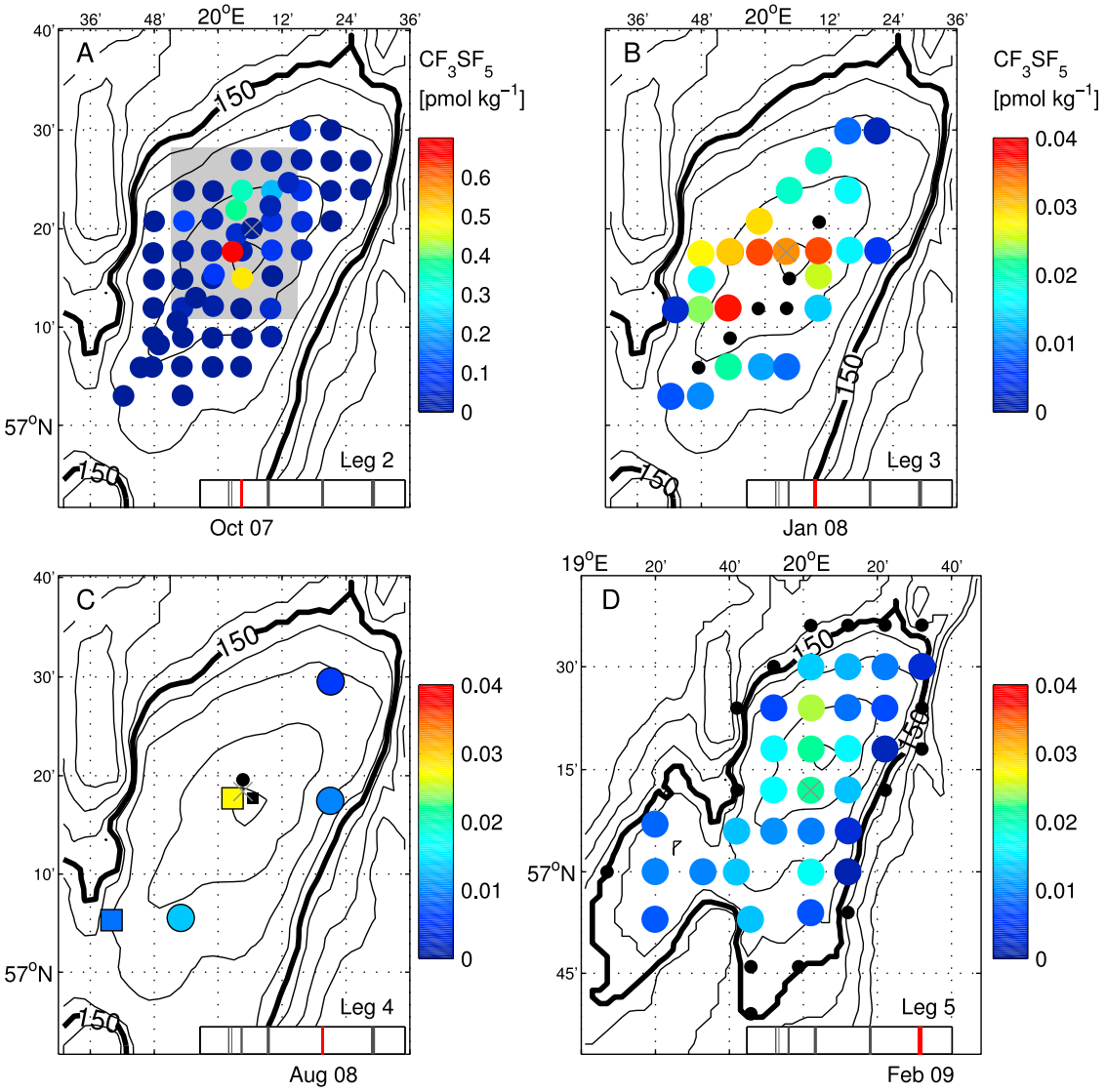

Figure 10. (a–d) Spatial distribution of tracer concentrations averaged between the bottom and 150 m depth (cruise dates are schematically indicated in the lower right). Note the different scale in Figure 10a and map area in Figure 10d. Crosses indicate positions of the densest profiles; black markers show profiles not covering the entire averaging range. Measurements at the central station in Figure 10c have been slightly shifted for better visibility. The gray rectangle in Figure 10a indicates the area shown in Figure 12.

and subsequent mixing have strongly reduced the initial patchiness of the tracer, suggesting, as a first important result, that lateral deep water dispersion occurs on a time scale of a few months. From these data it is also evident that onwards from some point between Legs 2 and 3, the tracer was in permanent contact with the lateral slopes of the basin, pointing at a possible influence of boundary mixing processes. The tracer concentrations for Leg 4/1 and Leg 4/2 are, despite the low number of samples and the time difference of approximately 40 days between the cruises, in remarkable agreement (Figure 8). This is consistent with Part 2, where we have investigated heat and salinity budgets from moored instrumentation, concluding that mixing during the summer months is generally weak.

[32] Overall, steadily decreasing tracer concentrations below 150 m depth are observed (Figures 7–9), indicating a net loss of tracer from the deep, enclosed part of the basin. Fluid above this level is topographically almost unconstrained (see Figure 1), suggesting that mixed-up tracer is likely to be advected across a large area of the Baltic Sea, and quickly diluted below the detection limit.

[33] The vertical concentration profiles shown in Figures 7–9 reveal a number of features that are rather different from tracer experiments conducted in the open ocean. The presence of lateral boundaries leads to an asymmetric vertical spreading around the tracer peak, and a gradual sinking of both the injection isopycnal (potential density: 9.92 kg m^{-3}) and the tracer peak. As shown below, this sinking mirrors the reduction of deep water density due to mixing rather than being related to any kind of vertical advection mechanism. After Leg 4, approximately 10 months after the injection, the injection isopycnal

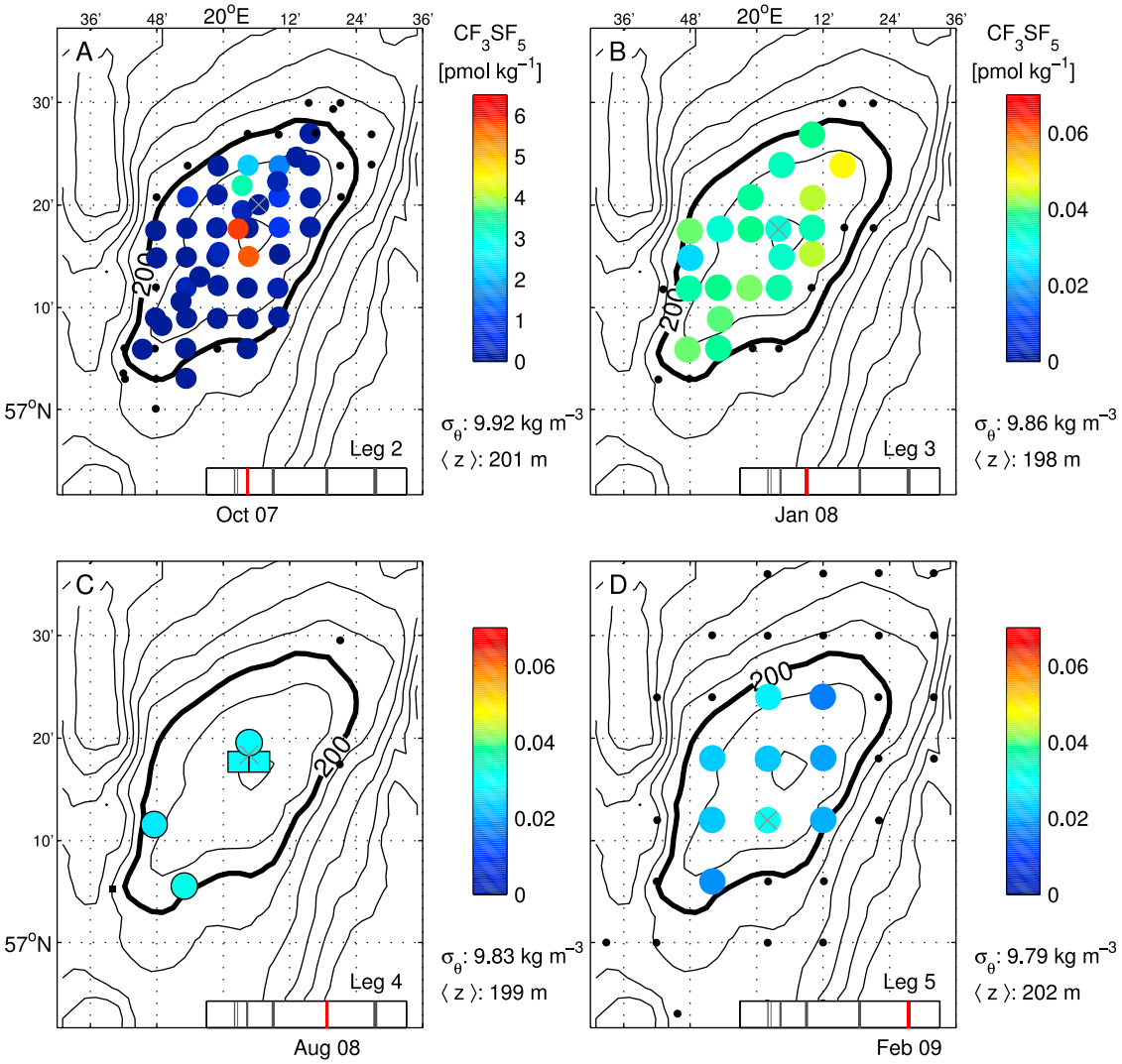

Figure 11. As in Figure 10 but for the tracer distribution on isopycnals located at approximately 200 depth (corresponding values of σ_θ as indicated). Isopycnal positions in density space are marked in Figures 6a, 7a, 8a, and 9a. Note the different scale in Figure 11a.

has reached the bottom, and could not be found anymore on subsequent cruises. As a consequence, a transition is observed from tracer profiles with a well-defined peak near the injection isopycnal (Figures 1, 6, and 7) toward profiles with concentrations increasing monotonically with depth (Figures 8 and 9).

6.2. Beyond the Gotland Basin

[34] In order to investigate the propagation of tracer beyond our study site in the Gotland Basin, Leg 5 also included tracer samples from a number of neighboring side basins, including the Fårö Deep (FD), the Landsort Deep (LD), the southwestern side basin (SB) of the Gotland Basin, and an unnamed location southwest of the island of Gotland (Figure 13). Tracer was detected in the deep water of all these stations, except southwest of Gotland, supporting the idea that deep water transport of dissolved matter may occur over considerable distances even during a stagnation period with no major inflow events.

[35] A comparison of tracer profiles from the Gotland Basin and the side basin SB (Figure 14) illustrates a nearly identical vertical distribution at overlapping depth intervals, suggesting a close communication between both basins. A likely mechanism explaining this similarity is that the frequently observed, strong isopycnal displacements described in Part 2 lift tracer from the Gotland Basin over the sill, where it subsequently intrudes in the form of dense gravity currents into the side basin. In spite of the shallower sill depth, a similar mechanism may have transported tracer also to the Fårö Deep, where comparable tracer concentrations were found in the same depth range, as well as in the Landsort Deep (LD), where significant tracer concentrations could only be identified in the lowest sample close to the bottom (Figure 14).

6.3. Tracer Statistics

[36] Following *Ledwell and Watson* [1991], some useful statistical characteristics of the tracer distribution can be

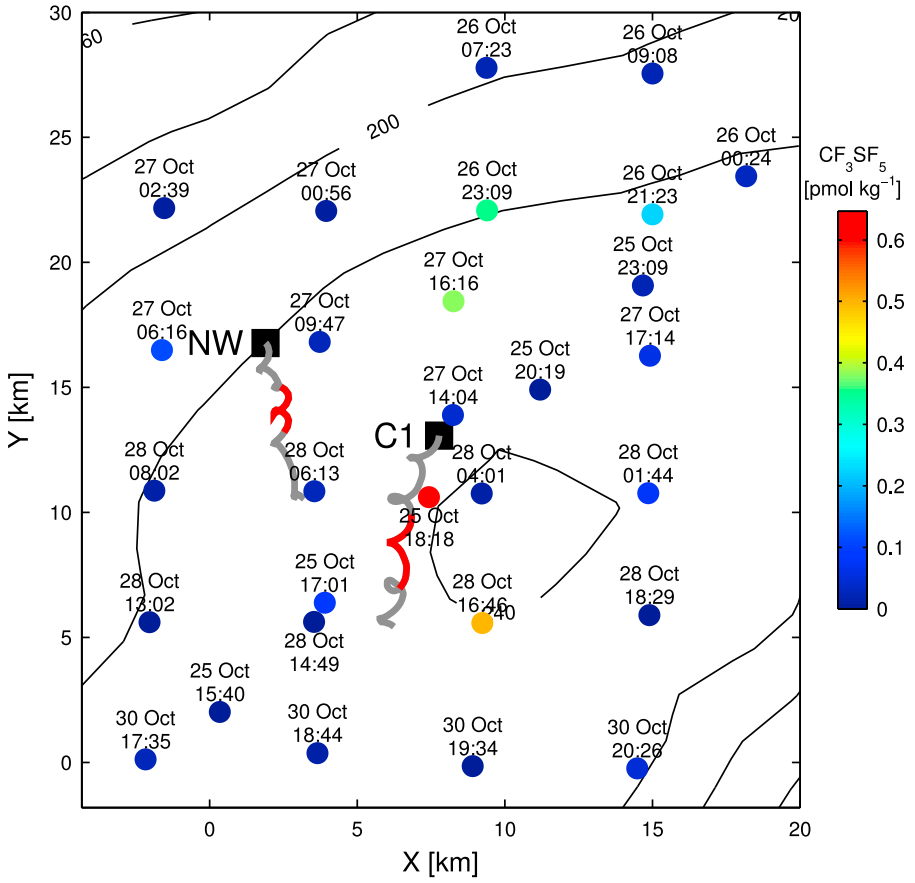

Figure 12. Enlarged view of central basin (area indicated in Figure 10a) with vertically averaged tracer concentrations during Leg 2 (exact sampling dates are indicated on top of each measurement). Positions of moorings NW and C1 are marked as black squares. Gray lines correspond to pseudotrajectories at 200 m depth for 2.9 days between 25 October (18:18 UTC) and 28 October (16:46 UTC); marked in red are 0.7 days between 26 October 2007 (23:09 UTC) and 27 October (16:16 UTC).

obtained by normalizing individual tracer samples. To this end, local concentrations c_{ij}, measured at depth z_i and lateral position $\mathbf{x}_j$, are divided by the mean concentration $\langle c_i \rangle$ at the same depth: $n_{ij} = c_{ij}/\langle c_i \rangle$. Consistent with the discussion of lateral variability in the previous section, the distribution of the n_{ij} for Leg 2 is strongly skewed, with a dominance of empty tracer samples ($n_{ij} = 0$), and few very high concentrations with $n_{ij} \gg 1$ (Figure 15a). This is contrasted by the histograms for Legs 3–5, exhibiting a symmetrical distribution around peak value near $n_{ij} = 1$ (Figures 15b–15d). Using the fact that these distributions are nearly Gaussian, we identify the uncertainty regions shown in Figures 7–9 with the respective standard deviations. For the highly non-Gaussian histogram of Leg 2 (see Figure 7), however, the uncertainty was computed based on the difference in profile shapes, as suggested by *Ledwell and Bratkovich* [1995].

7. Mixing Rates

7.1. Budget of Total Deep Water Tracer Mass

[37] The evolution of the total amount of tracer in the Gotland Basin is estimated here from the integral of the isopycnically averaged concentrations, taking the basin geometry into account

$$M = \int_{z_b}^{z_t} < c > A \, \mathrm{d}z, \tag{1}$$

where z_b denotes the position of the bottom, and z_t the upper integration limit, either $z_t = 170$ m or $z_t = 150$ m. In the latter case, the integration volume includes the side basin (SB) but not the Fårö Deep (see Figure 13). Recall that for Leg 2, tracer is found only in a few small patches, such that $\langle c \rangle$ is not representative for the whole basin area. In this case, the tracer mass M was calculated from the horizontal integral of the vertically integrated tracer concentrations. Uncertainties are computed from the standard deviations derived in the previous section, except for Leg 4, where the number of samples was not sufficient for reliable statistics.

[38] As discussed in section 6.1, it is quite likely that during Leg 2 advected small-scale tracer patches have been sampled twice at different grid points. To test the potential implications of this, the tracer mass for this cruise was estimated in two ways: (1) with the tracer concentrations as they were measured, and (2) with tracer concentrations excluding

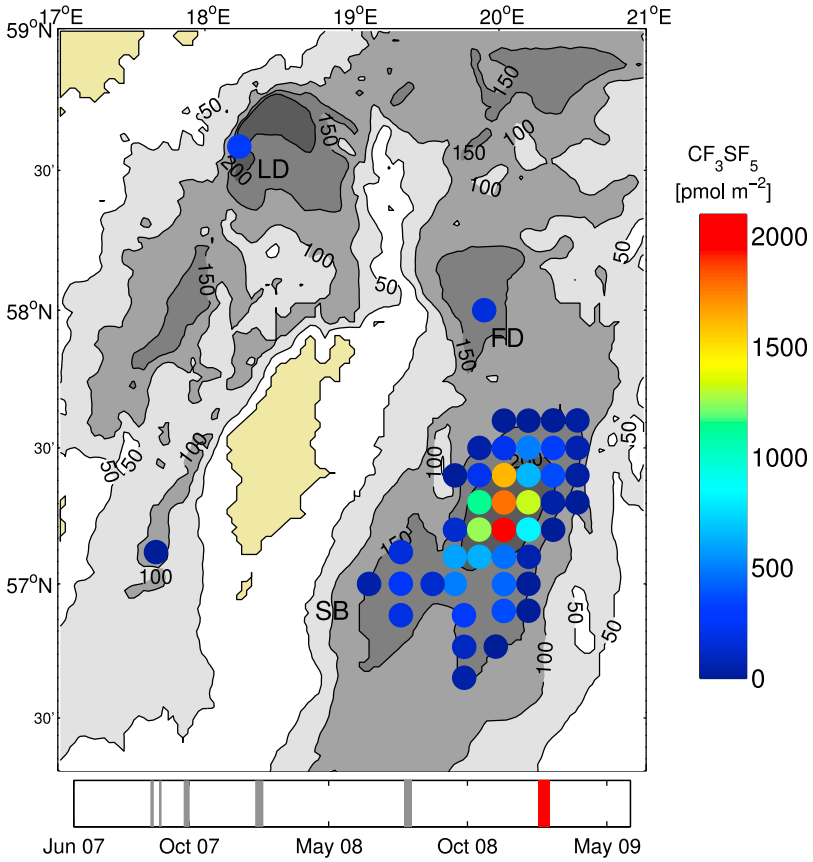

Figure 13. Vertically integrated tracer concentrations for Leg 5 (cruise date is indicated in the legend). All available measurements are shown, including those from the southwestern side basin (SB), from the Fårö Deep (FD), and from the Landsort Deep (LD).

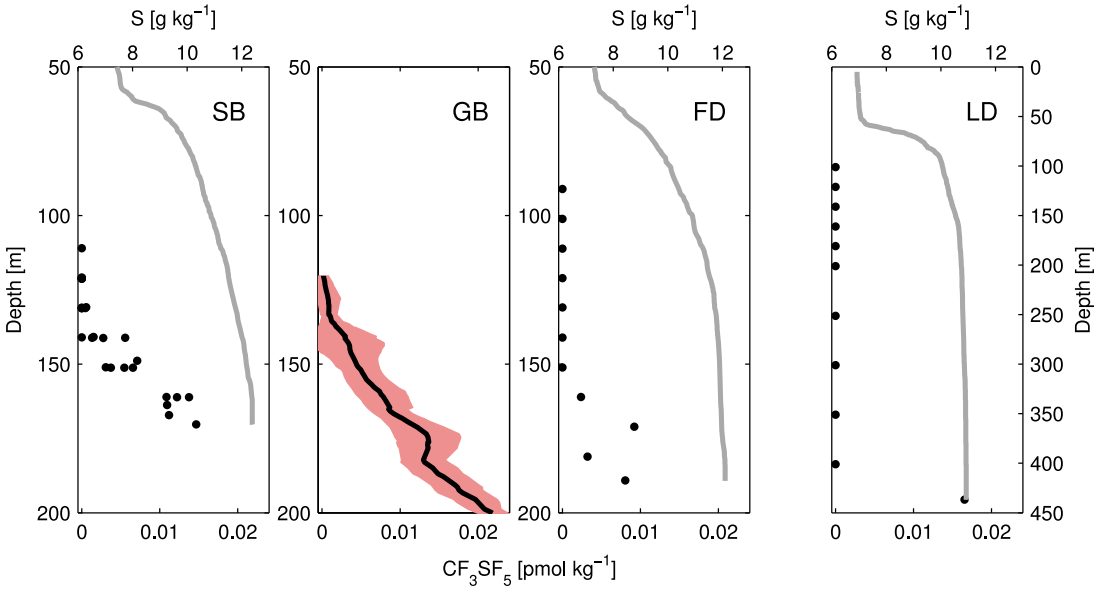

Figure 14. Tracer samples (black dots) and salinity profiles (gray) in the southwestern side basin (SB), Gotland Basin (GB), Fårö Deep (FD), and Landsort Deep (LD) for Leg 5 (514 DAI). The second figure shows the average tracer profile (black line, uncertainty in red) in the Gotland Basin.

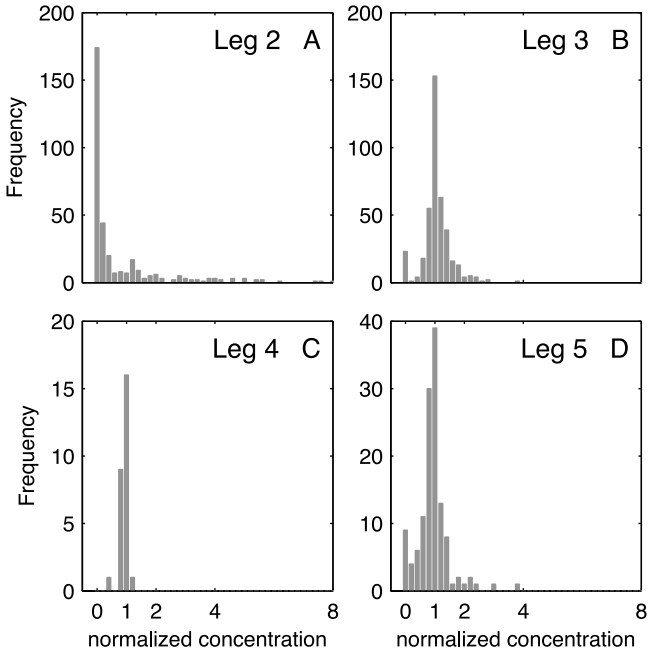

Figure 15. Histogram of normalized tracer concentrations n_{ij} for Legs 2–5.

profiles from 25 October (18:18) and 27 October (16:16), corresponding to tracer patches that were possibly measured a second time at different positions (see Figure 12 and discussion above). The estimated tracer masses for Legs 2–5 shown in Figure 16 illustrate the gradual loss of tracer in the deep water of the Gotland Basin due to vertical mixing followed by lateral advection out of the study area. For Leg 2, realistic (i.e., smaller than injected) values of M are obtained only if double counted profiles are excluded. The rate of tracer loss is seen to decrease with time, which should, however, not be misinterpreted as an indication for decreasing deep water mixing. This is for example evident from the fact that the stagnation of the total deep water tracer mass between Legs 3 and 4 is accompanied by a strong vertical tracer redistribution below 150 m depth (compare Figures 8 and 9), indicative for deep water mixing without net tracer loss to higher layers.

[39] At the end of the observation period (Leg 5, 514 DAI), approximately 2 of the injected 4.6 mol of CF_3SF_5 are still found in the study area below 150 m depth, including a small (7%) contribution from the southwestern side basin. Less than 5% of the tracer mass in the Gotland Basin are found in the Fårö Deep, which is, however, not included in the budget for the Gotland Basin. The exodus of tracer from the deep water is not very well approximated by an exponential decay law (Figure 16). Nevertheless, an e-folding time scale for deep water renewal of somewhat less than 2 years appears to be a useful first-order estimate.

7.2. Vertical Diffusivities

[40] From the lateral tracer distributions discussed in the context of Figures 10 and 11 above, we know that during the initial phase of the experiment the tracer had not been in intense contact with the lateral slopes of the basin. While for this initial period we expect that the observed vertical tracer spreading results mainly from interior mixing processes, during all subsequent cruises boundary mixing processes have to be taken into account. This different behavior is mirrored in different methods for the data analysis.

[41] In the first case (interior mixing), the presence of lateral boundaries may be ignored, and the analysis becomes

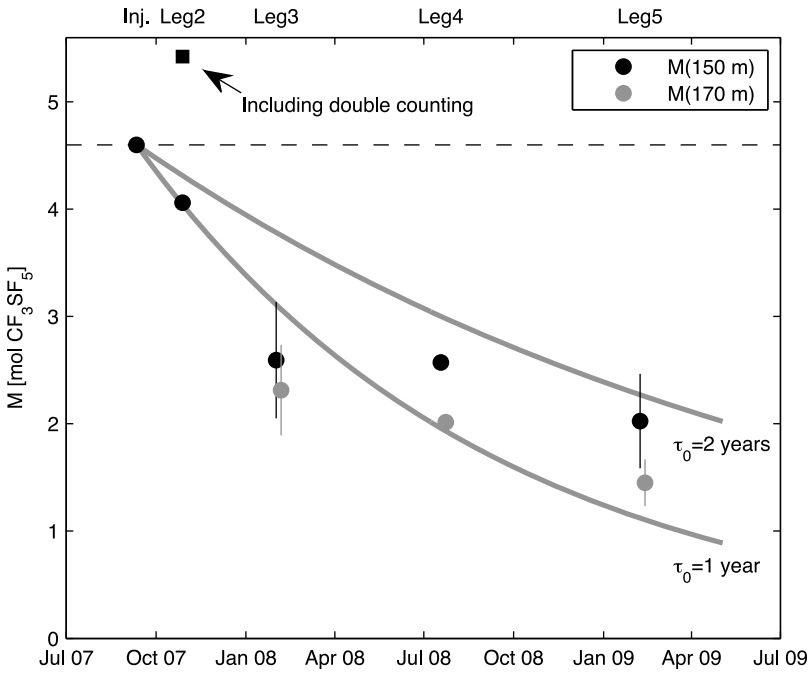

Figure 16. Total amount of tracer in the Gotland Basin below 170 m (gray) and below 150 m (black, including side basin). Gray curves correspond to exponential decay functions with time constants as indicated. The dashed line indicates the injected amount of 4.6 moles.

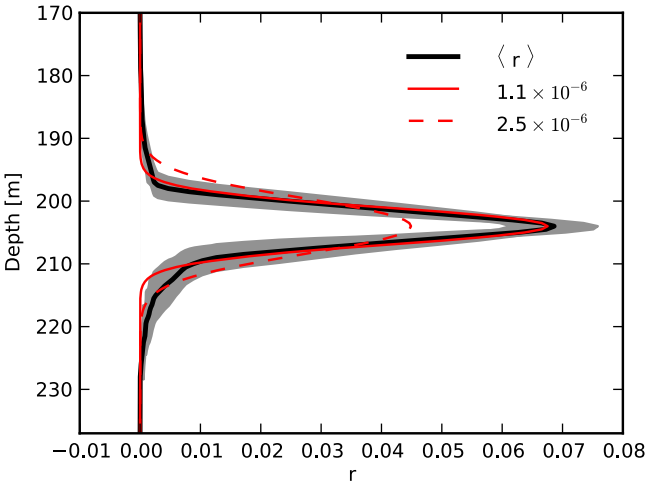

Figure 17. Normalized mean tracer concentration r for Leg 2 (black) with gray-shaded area including 1 standard deviation around the mean. In red are the profiles computed from the diffusion model (2) with different diffusivities as indicated in the legend.

identical to that used for tracer experiments in the open ocean. Here, as discussed by *Ledwell and Watson* [1991], it is advantageous to work with a normalized tracer profile, $r(z) = \langle c \rangle A/M$, where $\langle c(z) \rangle$ is the mean tracer concentration, and A an arbitrary but constant horizontal integration area, equal to or larger than the area with significant tracer concentrations. If isopycnal convergence is ignored (no lateral inflows), the normalized concentrations obey a diffusion equation of the form

$$\frac{\partial r}{\partial t} = \kappa_I \frac{\partial^2 r}{\partial h^2}, \tag{2}$$

where h is the distance from the tracer peak at the target density, and κ_I denotes the constant interior diffusivity. In discrete form, *Ledwell and Watson* [1991] suggest to compute $r_i = r(z_i)$ from the relation $r_i = \sum_j w_j c_{ij}/I_j$, where I_j denotes the vertical tracer integral at position $\mathbf{x}_j$. The weighting function is defined as $w_j = I_j/\sum_j I_j$.

[42] After isopycnal dispersion has brought the tracer in permanent contact with the lateral boundaries (this occurs at some time between Legs 2 and 3), boundary mixing processes cannot be ignored any longer. It can be shown that the transport equation describing the basin-scale vertical tracer transport in this case is of the form

$$A \frac{\partial < c >}{\partial t} = \frac{\partial}{\partial z} \left(A \kappa_{\mathrm{SF5}} \frac{\partial < c >}{\partial z} + A \bar{w} < c > \right) + c_{\mathrm{in}} \frac{\partial A \bar{w}}{\partial z}, \tag{3}$$

where $\kappa_{\mathrm{SF5}}(z)$ is the not necessarily constant effective basin-scale tracer diffusivity, including boundary processes, and $\bar{w}(z)$ the vertical advection velocity. The latter is used below to model the effect of lateral inflows (intrusions), where $c_{\mathrm{in}}(z)$ denotes the tracer concentration of intruding fluid (usually assumed to be zero). The basin geometry is taken into account with the help of the hypsographic relation for the basin area $A(z)$. Equations analogous to (3) describe the basin-scale vertical transport of salinity and temperature, where, for high Reynolds number flows and in the absence of double diffusive effects, the corresponding effective diffusivities for temperature, κ_θ, and salinity, κ_S, are expected to coincide with κ_{SF5}. In all cases, a zero flux boundary condition is applied at the bottom.

7.3. Interior Mixing Rates

[43] For the period between the injection and Leg 2 (interior mixing only), modeled concentration profiles $r(z)$ are computed from (2) for varying κ_I, using a delta distribution at $r(0)$ as the initial condition. The diffusion equation in (2) was discretized with a centered finite difference scheme with vertical resolution Δz = 0.5 m, and explicit time stepping. The "optimal" diffusivity was identified from these simulations as the value of κ_I minimizing the cost function

$$\chi(\kappa_I) = \int (r - \hat{r})^2 \mathrm{d}z, \tag{4}$$

where $\hat{r}$ is the measured normalized tracer distribution during Leg 2. Following *Ledwell and Watson* [1991], we compute the uncertainty in $\hat{r}(z_i)$ from the weighted standard deviation of the normalized tracer distribution: $\sigma_i = \sum_j w_j/(1 - w_j)(r_{ij} - r_i)^2$, where $r_{ij} = c_{ij}/I_j$. This has been shown to be a useful estimate for non-Gaussian tracer distributions.

[44] The results are summarized in Figure 17. The optimal diffusivity according to (4) was found to be $\kappa_I = 1.1 \times 10^{-6}$ m^2 s^{-1}, where the condition that the modeled profiles are within 1 standard deviation σ_i of the concentration at the tracer peak yields an uncertainty of 0.2×10^{-6} m^2 s^{-1} for κ_I. A similar computation for the period between Leg 1 to Leg 2 (33 days) yields 1.0×10^{-6} m^2 s^{-1}, where we have used the measured profile for Leg 1 as initial condition, instead of the delta distribution.

[45] To check the stability of this result, we also tested an alternative method that is based on the well-known fact that for a diffusion problem of the form (2), the second moment σ_z^2 of the vertical tracer distribution $r(z)$ increases at a rate proportional to the diffusivity [e.g., *Kundu and Cohen*, 2008]:

$$\frac{\mathrm{d}\sigma_z^2}{\mathrm{d}t} = 2\kappa_I. \tag{5}$$

With σ_z computed from the measured $\hat{r}(z)$ for Leg 2, this approach yields $\kappa_I = 2.5 \times 10^{-6}$ m^2 s^{-1} for the time interval between the injection and Leg 2. Visual inspection of the modeled tracer profile suggests, however, that this value is an upper limit for κ_I because part of the variance results from the higher spreading rates at the lower edge of the peak (Figure 6) that are indicative for the beginning impact of boundary mixing. We thus conclude that the interior diffusivity is close to 1×10^{-6} m^2 s^{-1}, and unlikely to exceed the threshold of 2.5×10^{-6} m^2 s^{-1}. These values are comparable to those found in a recent study by *van der Lee and Umlauf* [2011], who investigated interior mixing with the help of direct turbulence microstructure observations in a neighboring basin (Bornholm Basin), and identified shear from near-inertial waves and mesoscale motions as the primary source of mixing.

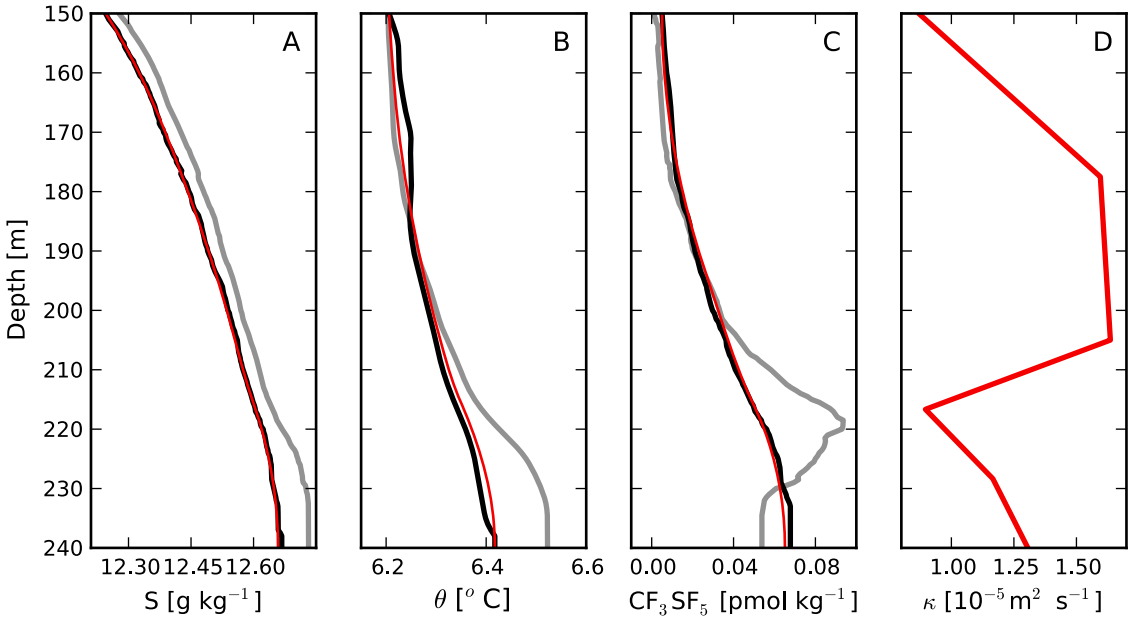

Figure 18. Profiles of (a) salinity, (b) potential temperature, and (c) tracer for Leg 3 (gray) and Leg 4 (black). (d) Modeled profiles based on the diffusivity shown in red.

7.4. Basin-Scale Mixing Rates

[46] Basin-scale vertical diffusivities for the periods between Legs 3 and 4 (150 days), and Legs 4 and 5 (224 days) were estimated with the help of the transport equation in (3), including hypsography but assuming that lateral intrusions have no significant effect on the tracer spreading ($\bar{w} = 0$). The latter is confirmed by the long-term observations from moored instrumentation described in Part 2. The period between Leg 2 and 3 turned out to be more complex due to the transition from interior to boundary mixing as discussed in section 7.5.

[47] For the period between Legs 3 and 4, we numerically solved (3) for the tracer concentrations, as well as two analogous equations for the isopycnically averaged potential temperatures and salinities, assuming $\bar{w} = 0$ in all cases. A Dirichlet-type boundary condition at the top of the integration volume (150 m) was derived for each of these variables by linearly interpolating between the observed values at the start and end of the integration period, respectively. Identical basin-scale diffusivities were assumed: $\kappa_{SF5} = \kappa_S = \kappa_\theta$. Optimal diffusivity profiles were obtained by minimizing the cost functions for T, S, and tracer (with equal weights), now, however, allowing for vertically variable diffusivities. The latter is realized by introducing additional degrees of freedom by letting κ vary at 6 vertical positions (values between these positions are interpolated linearly onto the numerical grid). For the optimization, we use the algorithm described by *Byrd et al.* [1995] to efficiently handle the large number of degrees of freedom in this problem.

[48] The results of this analysis are depicted in Figures 18 and 19. The solution of (3) with diffusivities optimized as described above is seen to lead to excellent agreement between observations and model results for all three variables. Diffusivities are on the order of 10^{-5} m^2 s^{-1}, and therefore approximately 1 order of magnitude larger than the interior diffusivities discussed in the previous section. This dramatic increase in mixing rates cannot be explained by differences in wind forcing because wind speeds between Legs 2 and 3 were on the average substantially larger than those between Legs 3 and 4 (Part 2). It is, however, very likely that the strongly increased mixing rates reflect the effect of boundary mixing, consistent with the observation that during the whole period from Leg 3 to Leg 5 the tracer was in contact with the boundaries, whereas before Leg 2 this was not the case. This forms one of the main conclusion of this paper.

[49] As shown in Figures 18d and 19d, diffusivity profiles for different periods exhibit similar vertical structures with high values in the bottom boundary layer (BBL), a local minimum at 220–230 m depth, and increasing values in the layer above (note that the structure of the diffusivities inside and at the top of the BBL is not resolved with only 6 degrees of freedom in the vertical). This increase in diffusivities above 220 m is also consistent with diffusivities computed from deep water budgets for heat and salinity, using long-term moored CTD chains at C1 as discussed in more detail in Part 2. However, the inclusion of vertical variability is not essential for obtaining acceptable fits between modeled and observed profiles. We have also optimized the problem with constant diffusivities (not shown), which still leads to good fits, and results in diffusivities of 1.3×10^{-5} m^2 s^{-1} for the period between Legs 3 and 4, and 1.9×10^{-5} m^2 s^{-1} for Legs 4 and 5.

7.5. Transition From Interior to Basin-Scale Mixing

[50] While the results for Legs 3 to 5 suggest that the evolution of tracer, temperature, and salinity can be described rather accurately with the help of a one-dimensional diffusion model using identical diffusivities for all three variables, this was not the case for the period between Legs 2 and 3. This period was characterized by a transition from interior

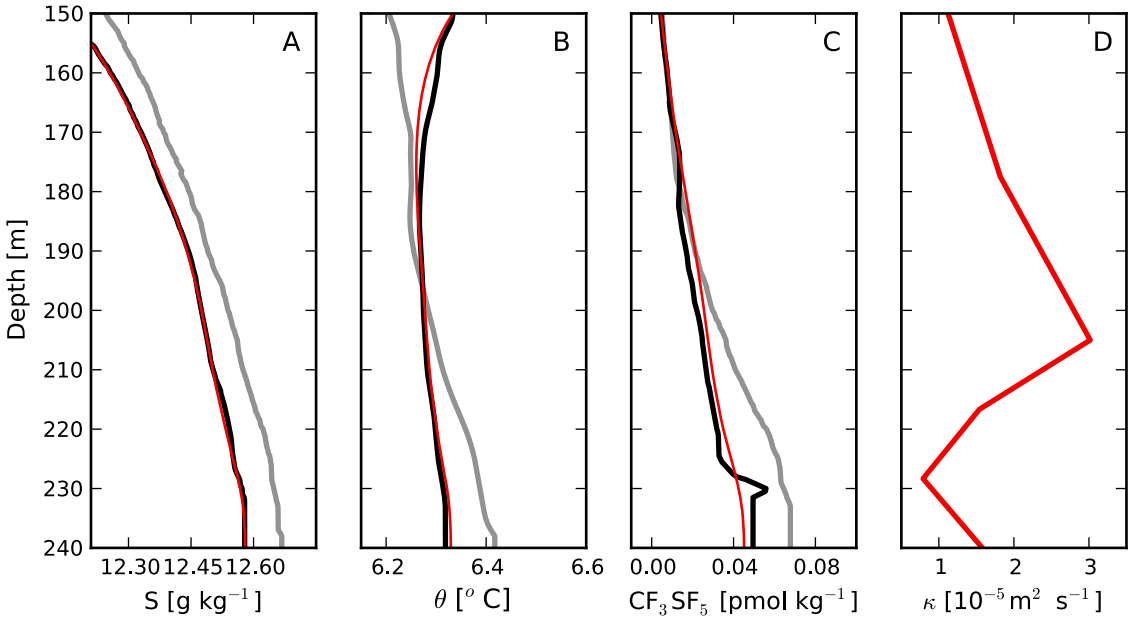

Figure 19. As in Figure 18 but for the period between Leg 4 (gray) and Leg 5 (black).

to boundary mixing during which additional processes may have affected the tracer spreading in different ways.

[51] In order to illustrate the problem, we discard the assumption of identical diffusivities for all quantities, still assuming, however, that lateral intrusions are absent: $\bar{w} = 0$ in (3). In contrast to Legs 3 to 5 described above, now the tracer diffusivity κ_{SF5} is optimized independently of $\kappa_\theta = \kappa_S$ used to model the evolution of θ and S. Figures 20a and 20b illustrate that with these additional assumptions, the diffusion model yields good agreement between measured and modeled profiles for temperature and salinity. The corresponding diffusivity κ_θ is a few times 10^{-5} m^2 s^{-1}, somewhat larger than the values found for Legs 3 to 5 but still plausible because the period between Legs 2 and 3 corresponds to the stormy winter months October–January (as shown in Part 2, diffusivities derived from salinity and temperature budgets show a similar increase during the winter months). Again, the vertical structure of κ_θ with a minimum at 220–230 m depth is similar to the tracer profiles shown in Figures 18d and 19d above.

[52] However, as shown in Figure 20d, the diffusivities κ_{SF5} and κ_θ exhibit completely different vertical structures, locally differing by more than an order of magnitude. As a result, using κ_{SF5} to model θ and S, or vice versa κ_θ to model the tracer profile, completely unrealistic profiles are obtained (Figures 20a–20c), indicating that the description of the problem as a pure diffusion process is an over simplification during the transition phase.

[53] We have investigated several alternative processes that may have caused the strong vertical redistribution of tracer between Legs 2 and 3, and the associated tracer loss to higher layers. The possibility of tracer loss due to particle adsorption and sinking to the sediment can be excluded because: (1) comparison of Figures 6a and 7a shows no evidence for a relative motion between the tracer peak and the target isopycnal ($\sigma_\theta = 9.92$ kg m^{-3}) and (2) Figure 7 suggests that tracer concentrations *decrease* toward the sediment, contrary to what would be expected if a large part of the tracer had sunk to the sediment surface. We have also examined the potential effect of deep water renewal due to small lateral intrusions that may have remained undetected in temperature and salinity. This was motivated by the observation that interleaving of tracer-free fluid into layers above the tracer peak could have resulted in the observed strong reduction of concentrations, and in an advective tracer loss across the upper boundary of the control volume due to isopycnal divergence. For these investigations, we have solved equation (3), assuming different configurations with $\bar{w} \neq 0$ and $c_{in} = 0$ in order to mimic the effect of intrusions. Observed tracer profiles could only be reproduced if the intruding fluid volume was of the order of the total deep water volume, or, in other words, if a major deep water inflow had occurred. It is highly unlikely that such an event would have remained unnoticed in both our CTD data and the moorings described in Part 2.

[54] In the following, we suggest that the failure of the diffusion model is based on its inability to represent nonlocal transport effects during the transition phase. To this end, it should be recalled that "boundary mixing" involves a number of subprocesses essential for the overall basin-scale effect: (1) smoothing of cross-slope gradients inside the BBL (this is the actual boundary mixing process); (2) exchange of fluid between the BBL and the interior; and (3) homogenization of isopycnal tracer variability in the interior. If the time scales of processes 2 and 3 are small compared to 1, only small isopycnal concentration differences are expected between the interior and the BBL (Figure 21a), implying that diapycnal gradients in the BBL and the interior are nearly identical. In this case, cross-slope mixing in the BBL determines the basin-scale vertical transport. Contrary, if upslope mixing in the BBL occurs much faster than the exchange processes 2 and 3, isopycnal concentrations gradients build up between the BBL and the interior. Via intrusions, these gradients drive an isopycnal

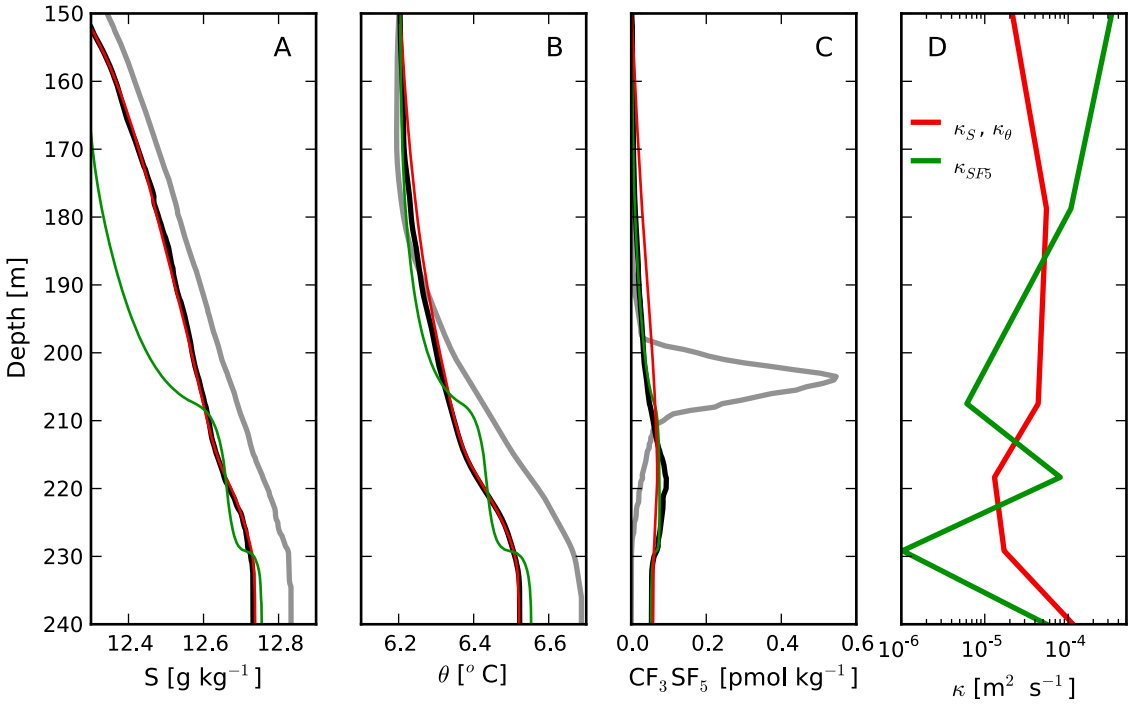

Figure 20. Profiles of (a) salinity, (b) potential temperature, and (c) tracer for Leg 2 (gray) and Leg 3 (black). Red and green curves in Figures 20a–20c represent model results using (d) the corresponding diffusivities.

tracer flux q_c between the BBL and the interior that may have no relation to the local vertical tracer gradient in the interior (Figure 21b). The bottle neck for basin-scale vertical transport in this case is the exchange between BBL and interior, rather than cross-slope mixing inside the BBL, which constitutes a *nonlocal* transport mechanism that cannot be described by a diffusion model based on *local* mean gradients. For example, tracer may leave the basin via the BBL without being noticed in the interior, which may explain the strong tracer loss between Legs 2 and 3.

[55] Support for this hypothesis comes from Figure 7 (Leg 3), in which tracer samples taken within 2 m distance from the bottom are marked in green. BBL concentrations near the tracer peak are seen to be consistently smaller than the isopycnal average, whereas concentrations higher up in the water column show the opposite behavior. In agreement with the schematic view in Figure 21b, this suggests that tracer is lost from the interior toward the BBL near the tracer peak, diffused upslope inside the BBL, and finally injected into higher layers. The separation between the two regions is located around 210 m depth. The effect is even more pronounced for Leg 2 (Figure 6), where data suggest that the asymmetric downward spreading of the tracer (higher concentrations below the peak than above) is an indication for the beginning influence of boundary mixing. It is therefore likely that isopycnal concentration differences between the BBL and the interior characterize the whole transition period between Legs 2 and 3.

8. Conclusions

[56] Apart from the pilot study by *Ho et al.* [2008], the tracer compound CF_3SF_5 which our experiment was based on has not been previously used in TREs, and only limited knowledge is available about its performance in real ocean applications. In our case, the tracer has proven to be long-term stable with no discernible sinking effects due to particle adsorption, and no indications for chemical decay even under permanently anoxic conditions with high concentrations of H_2S. This forms a solid basis for future experiments.

[57] As one of the key results of our study, the different spreading rates observed before and after the tracer was in contact with the lateral slopes of the basin provide strong evidence for the importance of boundary mixing. Similar to previous studies in fjords [*Stigebrandt*, 1979], stratified lakes [*Goudsmit et al.*, 1997; *Becherer and Umlauf*, 2011],

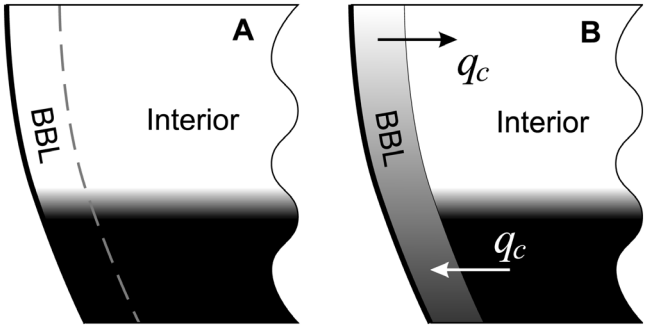

Figure 21. Schematic view of tracer concentrations (in gray) in a stratified basin with (a) slow upslope mixing inside BBL, or rapid exchange between BBL and interior, and (b) rapid upslope mixing inside BBL, or slow exchange between BBL and interior (q_c indicates the isopycnal tracer flux between the BBL and the interior).

and ocean basins [*Ledwell and Hickey*, 1995; *Ledwell and Bratkovich*, 1995], we find an order of magnitude difference between interior and basin-scale effective diffusivities. While this suggests a qualitative similarity between the different experiments, it should be noted that the diffusivities found in the Gotland Basin (interior: $\sim 10^{-6}$ m^2 s^{-1}, basin-scale: $\sim 10^{-5}$ m^2 s^{-1}) are an order of magnitude smaller than the corresponding values found by *Ledwell and Hickey* [1995] for the Santa Monica Basin. In contrast to this, horizontal diffusitives in the Gotland Basin, estimated from lateral tracer spreading rates following the variance method described by *Ledwell and Watson* [1991], were of the order of 10 m^2 s^{-1} on a 10 km scale, and thus comparable to the Santa Monica Basin. It is likely that the discrepancy in vertical mixing rates mirrors the different mixing mechanisms and energy levels near the lateral slopes. *Ledwell and Hickey* [1995] speculate, e.g., that the critical reflection of internal tides at sloping topography may be an important energy source for boundary mixing, different from the virtually tideless Baltic Sea. The observation of *van der Lee and Umlauf* [2011] that interior internal wave mixing cannot explain basin-scale mixing rates in a neighboring deep basin, as well as the analysis of turbulence microstructure data discussed in Part 2 provide further support for the importance of boundary mixing.

[58] Finally, it is important to note that the dominance of boundary mixing implies that the observed tracer spreading in the interior is a result of isopycnal motions (intrusions) associated with the exchange of boundary layer and interior fluid. Our results have shown that the physical mechanisms governing these exchange processes may be crucial for the basin-scale vertical distribution of matter. These processes are not well understood at the moment, pointing at future work.

[59] **Acknowledgments.** We like to thank the crews and fellow scientists on board R/V *Prof. A. Penck*, R/V *Alkor*, R/V *Merian* and R/V *Poseidon* for their invaluable support. Special thanks to Jim Ledwell, Stew Sutherland, and Brian Guest for support with the OTIS, Siegfried Krüger and Volker Mohrholz for technical support, and Katrin König for coordinating the tracer sampling during one of the surveys. The project was financed by the German Research Foundation (DFG) under grants UM79/3-1, UM 79/4-1, and TA 317/1-1.

References

Axell, L. (1998), On the variability of Baltic Sea deepwater mixing, *J. Geophys. Res.*, *103*(C10), 21,667–21,682.

Barber, C., D. Dobkin, and H. Huhdanpaa (1996), The Quickhull algorithm for convex hulls, *ACM Trans. Math. Software*, *22*(4), 469–483.

Becherer, J., and L. Umlauf (2011), Boundary mixing in lakes: 1. Modeling the effect of shear-induced convection, *J. Geophys. Res.*, *116*, C10017, doi:10.1029/2011JC007119.

Bullister, J. L., and B. S. Lee (1995), Chlorofluorocarbon-11 removal in anoxic marine waters, *Geophys. Res. Lett.*, *22*, 1893–1896.

Bullister, J. L., and R. F. Weiss (1988), Determination of CCl3F and CCl2F2 in seawater and air, *Deep Sea Res. Part I*, *35*(5), 839–853.

Byrd, R. H., P. Lu, and J. Nocedal (1995), A limited memory algorithm for bound constrained optimization, *SIAM J. Sci. Stat. Comput.*, *16*(5), 1190–1208.

Feistel, R., G. Nausch, and N. Wasmund (Eds.) (2008), *State and Evolution of the Baltic Sea, 1952–2005. A Detailed 50-Year Survey of Meteorology and Climate, Physics, Chemistry, Biology, and Marine Environment*, 703 pp., Wiley-Interscience, Hoboken, N. J.

Ho, D. T., J. R. Ledwell, and W. M. Smethie (2008), Use of SF_5CF_3 for ocean tracer release experiments, *Geophys. Res. Lett.*, *35*, L04602, doi:10.1029/2007GL032799.

Goudsmit, G.-H., F. Peeters, M. Gloor, and A. Wüest (1997), Boundary versus internal diapycnal mixing in stratified natural waters, *J. Geophys. Res.*, *102*(C13), 27,903–27,914.

Gustafsson, B. G., and A. Stigebrandt (2007), Dynamics of nutrients and oxygen/hydrogen sulfide in the Baltic Sea deep water, *J. Geophys. Res.*, *112*, G02023, doi:10.1029/2006JG000304.

Holtermann, P. L., and L. Umlauf (2012), The Baltic Sea Tracer Release Experiment: 2. Mixing processes, *J. Geophys. Res.*, *117*, C01022, doi:10.1029/2011JC007445.

Krysell, M., E. Fogelqvist, and T. Tanhua (1994), Apparent removal of the transient tracer carbon tetrachloride from anoxic seawater, *Geophys. Res. Lett.*, *21*, 2511–2514.

Kullenberg, G. (1977), Observations of the mixing in the Baltic thermo- and halocline layers, *Tellus*, *29*, 572–587.

Kundu, P. K., and I. M. Cohen (2008), *Fluid Mechanics*, 4 ed., 872 pp., Academic, San Diego, Calif.

Ledwell, J. R., and A. Bratkovich (1995), A tracer study of mixing in the Santa Cruz Basin, *J. Geophys. Res.*, *100*, 20,681–20,704.

Ledwell, J. R., and B. M. Hickey (1995), Evidence for enhanced boundary mixing in the Santa Monica Basin, *J. Geophys. Res.*, *100*, 20,665–20,679.

Ledwell, J. R., and A. J. Watson (1991), The Santa Monica Basin Tracer Experiment: A study of diapycnal and isopycnal mixing, *J. Geophys. Res.*, *95*, 8695–8718.

Ledwell, J. R., A. J. Watson, and C. S. Law (1998), Mixing of a tracer in the pycnocline, *J. Geophys. Res.*, *103*(C10), 21,499–21,529.

Ledwell, J. R., L. C. St. Laurent, J. B. Girton, and J. M. Toole (2011), Diapycnal Mixing in the Antarctic Circumpolar Current, *Journal of Physical Oceanography*, *41*, 241–246.

Reissmann, J., H. Burchard, R. Feistel, E. Hagen, H.-U. Lass, V. Mohrholz, G. Nausch, L. Umlauf, and G. Wieczorek (2009), Vertical mixing in the Baltic Sea and consequences for eutrophication—A review, *Progr. Oceanogr.*, *82*, 47–80.

Schneider, B., G. Nausch, and C. Pohl (2010), Mineralization of organic matter and nitrogen transformations in the Gotland Sea deep water, *Mar. Chem.*, *119*, 153–161.

Stigebrandt, A. (1979), Observational evidence for vertical diffusion driven by internal waves of tidal origin in the Oslofjord, *J. Phys. Oceanogr.*, *9*(2), 435–441.

Strady, E., C. Pohl, E. V. Yakushev, S. Krüger, and U. Hennings (2008), Pump-CTD-system for trace metal sampling with a high vertical resolution. A test in the Gotland Basin, Baltic Sea, *Chemosphere*, *70*(7), 1309–1319.

Tanhua, T., and K. A. Olsson (2005), Removal and bioaccumulation of anthropogenic, halogenated transient tracers in an anoxic fjord, *Mar. Chem.*, *94*, 27–41.

Tanhua, T., E. Fogelqvist, and Ö. Bastürk (1996), Reduction of volatile halocarbons in anoxic seawater, results from a study in the Black Sea, *Mar. Chem.*, *54*, 159–170.

Umlauf, L., T. Tanhua, J. J. Waniek, O. Schmale, P. Holtermann, and G. Rehder (2008), Hunting a new ocean tracer, *EOS Trans. AGU*, *89*(43), 419–420.

van der Lee, E. M., and L. Umlauf (2011), Internal-wave mixing in the Baltic Sea: Near-inertial waves in the absence of tides, *J. Geophys. Res.*, *116*, C10016, doi:10.1029/2011JC007072.

Watson, A. J., and J. R. Ledwell (2000), Oceanographic tracer release experiments using sulphur hexafluoride, *J. Geophys. Res.*, *105*(C6), 14,325–14,337.

Winters, K. B., P. N. Lombard, J. J. Riley, and E. A. D'Asaro (1995), Available potential energy and mixing in density-stratified fluids, *J. Fluid. Mech.*, *289*, 115–128.

P. L. Holtermann, G. Rehder, O. Schmale, L. Umlauf, and J. J. Waniek, Leibniz Institute for Baltic Sea Research, Seestr. 15, D-18119 Warnemünde, Germany. (lars.umlauf@io-warnemuende.de)

T. Tanhua, Leibniz Institute for Marine Sciences, Düsternbrooker Weg. 20, D-24105 Kiel, Germany.